have been raised; transport may be mediated through vesicles, through complex membrane networks, non-lipid enclosed protein aggregates, or lipid enclosed structures such as Maurer's clefts [4,15].

A few hundred proteins are known to contain a PEXEL/VTS motif, defining a large *Plasmodium* exportome [9,16]. However, several parasite proteins that are transported to the iRBC lack both an N-terminal signal sequence and a PEXEL/VTS motif, and are termed "PEXEL negative exported proteins" (PNEPs) [17]. The most well characterized PNEPs are skeleton-binding protein 1 (SBP1) [18], the membrane associated histidine-rich protein 1 (MAHRP1) [19] and the ring-exported proteins 1 (REX1) and 2 (REX2) [17,20,21]. Most of the reported PNEPs are believed to be trafficked to the iRBC *via* the classical secretory pathway, involving initial transport to the ER, but no shared signal or transport-related sequence has been identified to date for subsequent transport to the iRBC. SBP1, MAHRP1 and REX2 lack a signal peptide but contain a transmembrane (TM) region which, along with sequences at their N-terminal region, has been implicated in protein transport [22–24]; however, the hydrophobic N-terminal region of the REX1 protein has been shown to be the only region required for transport of this particular protein [25].

The recently identified *P. falciparum* surface-associated interspersed gene (*surf*) family encodes high molecular mass proteins, and one of these, SURFIN$_{4.2}$, has been shown to be co-transported along with *Pf*EMP1 and RIFIN to the iRBC surface [26]. The N-terminal of SURFIN$_{4.2}$, predicted to be extracellular, contains a moderately conserved cysteine-rich putative globular domain (CRD) preceding a variable segment (Var) followed by a putative TM region. The C-terminal region of SURFIN$_{4.2}$ contains three tryptophan-rich (WR) domains which are highly conserved among SURFIN protein members, intersected by stretches of higher variability. The protein does not appear to contain either a hydrophobic signal peptide sequence or a classical PEXEL motif. Although there are two PEXEL-like sequences located at the N-terminal segment amino acid positions (aa) 24–30 (R_KI_FE) and aa 118–122 (R_TL_ED), they may not be true signals because the first does not completely agree with the consensus PEXEL motif, and the second was located in the putative globular domain CRD. This suggests that SURFIN$_{4.2}$ may be transported *via* a PEXEL-independent pathway. Using a serial deletion approach, we have attempted to identify the regions involved in *P. falciparum* SURFIN$_{4.2}$ transport into the iRBC. We generated a panel of transgenic parasite lines expressing green fluorescent protein (GFP)-tagged recombinant SURFIN$_{4.2}$ and show that the protein is trafficked as a PNEP. We show that the TM region, the only predicted hydrophobic region of the protein, is necessary for entry into the parasite's secretory pathway and for subsequent trafficking into the iRBC. These findings confirm the importance of hydrophobic regions for the trafficking of PNEPs.

2. Materials and methods

2.1. Plasmid construction

A panel of plasmids that were used to make final *P. falciparum* transfection constructs were prepared based on the Multisite Gateway® system (Invitrogen, Carlsbad, CA) [27]. DNA fragments containing attB1 and attB2 sites were inserted into pUC19, resulting the pB12 plasmid. DNA fragments encoding aa 1–419 of SURFIN$_{4.2}$ (CRD and a part of Var), a triple HA tag, and aa 734–764 of SURFIN$_{4.2}$ (TM) were ligated into pB12 to make the pB12-SURF$_{4.2}$CRD-Var1-HA-TM plasmid. DNA fragments encoding aa 765–1347, 1320–1728 or 1712–2380 of SURFIN$_{4.2}$ (first, second or third WR domain) were ligated into pB12-SURF$_{4.2}$CRD-Var1-HA-TM, resulting in the pB12-SURF$_{4.2}$CRD-Var1-HA-TM-WR1, pB12-SURF$_{4.2}$CRD-Var1-HA-TM-WR2 or pB12-SURF$_{4.2}$CRD-Var1-HA-TM-WR3, respectively. DNA fragments encoding 50 amino acids at aa 684–734 adjacent to TM region, a triple HA tag, TM, and WR1 regions were ligated into pB12, resulting in the pB12-SURF$_{4.2}$VarC-HA-TM-WR1. All DNA fragments were amplified from *P. falciparum* 3D7 line parasites using KOD Plus DNA polymerase (Toyobo). pB12-SURF$_{4.2}$CRD-Var1-TM was further modified by site-directed mutagenesis using oligonucleotides with desired modifications as follows: To abolish the PEXEL-like sequences at aa 25–29 ($R_{25K}I_{27F}E_{29}$) or aa 118–122 ($R_{118T}L_{120E}D_{122}$), these sequences were replaced to $A_{25K}A_{27F}A_{29}$ or $A_{118T}A_{120E}A_{122}$, respectively, yielding pB12-SURF$_{4.2}$CRD-Var1-HA-TM-Pexel-1mut or pB12-SURF$_{4.2}$CRD-Var1-HA-TM-Pexel-2mut. To assess the N-terminal sequence for the trafficking, the N-terminal region at aa 1–42 (M_1LFVVELDSRLEKSADKRISVERFRKIFEIYVEDKLEELKRS$_{42}$) of SURFIN$_{4.2}$ was replaced with the N-terminal region at aa 1–15 (M_1DVHVNQLKNISPID$_{15}$) of *P. falciparum* adenylosuccinate lyase (ASL, PFB0295w), a *P. falciparum* enzyme not considered to be transported to the iRBC, to yield pB12-SURF$_{4.2}$CRD-Var1-HA-TM-RepN. pB12-SURF$_{4.2}$-Var1-HA-TM and pB12-SURF$_{4.2}$CRD-HA-TM were generated from pB12-SURF$_{4.2}$CRD-Var1-TM by removing a region encoding aa 46–196 containing the CRD and a region encoding aa 198–419 containing the Var1 region, respectively. These pB12-based plasmids were subjected to a BP recombination reaction with pDONR™221 (Invitrogen) according to the manufacturer's instructions, resulting in the corresponding pENT12 Gateway Entry vectors. These pENT12-based plasmids were then subjected to a Gateway MultiSite LR recombination reaction with other Entry vectors, *Pf*CRT 5′-pENTR4/1 (as a promoter component) and GFPm2-pENTR2/3 (as a tag sequence), and a Destination vector, pCHDR-3/4 (kind gifts from D. G McFadden), according to the manufacturer's instruction [27]. Initially, we used the promoter region of SURFIN$_{4.2}$, however, the signal was very weak, thus we decided to use CRT (chloroquine resistance transporter; MAL7P1.27) promoter, which has been used to study *P. falciparum* protein trafficking to the iRBC cytosol and Maurer's clefts, to overexpress recombinant proteins for the visualization of their clear location. Previous transcriptome data indicated that the promoter activity of CRT was stronger than that of SURFIN$_{4.2}$ and that CRT was mainly transcribed at schizont, ring, and early trophozoite stages, slightly longer than SURFIN$_{4.2}$ which was mainly transcribed at schizont and early ring stages. [28,29]. Obtained plasmids were verified by their restriction enzyme digestion pattern and sequencing. Schematic structures of the recombinant proteins expressed from the episomal form of the plasmids in the transfected *P. falciparum* are shown in Fig. 1. Detailed information may be found in Supplementary material.

2.2. Parasite culture and transfection

The *P. falciparum* MS822 line was used in this study. This line was isolated in Mae Sot, Thailand in 1988, maintained in vitro for less than 3 months, and kept at the Institute of Tropical Medicine, Nagasaki University [30]. Parasites were cultured in RPMI-1640 medium containing 5% heat-inactivated pooled type AB human serum and 0.25% Albumax II (Invitrogen), 200 mM hypoxanthine (SIGMA, St. Louis, MO), 10 μg/mL gentamycin (Invitrogen) and human RBC (type O) at 2% hematocrit. Human RBCs and plasma were obtained from the Nagasaki Red Cross Blood Center. Serum was produced from the acid–citrate–dextrose-containing plasma by removing the clot that had formed after adding calcium. *P. falciparum* transfection was performed essentially as previously described [31]. Briefly, RBCs were resuspended in 400 μL of incomplete Cytomix (120 mM KCl, 0.15 mM $CaCl_2$, 2 mM EGTA, 5 mM $MgCl_2$, 10 mM K_2HPO_4/KH_2PO_4, and 25 mM Hepes) containing 100 μg of plasmid DNA. Electroporations were performed in 2 mm cuvette using a Gene Pulser Xcell Electroporation System (Bio-Rad, Hercules, CA) with a condition of 320 mΩ, 0.32 kV and 975 μF. Observed time constants were 15–30 ms. Parasites were synchronized to ring stage by 5% sorbitol treatment, then 40 h later, mature trophozoites/schizonts-iRBCs were resuspended with the plasmids-preloaded RBCs (final 0.2% parasitemia). At day 3 post transfection, 5 nM of the anti-folate drug WR99210 (kind gift from Dr. D. Jacobus) was supplied to the culture medium, and was maintained until drug-resistant parasites reappeared. Resistant parasites

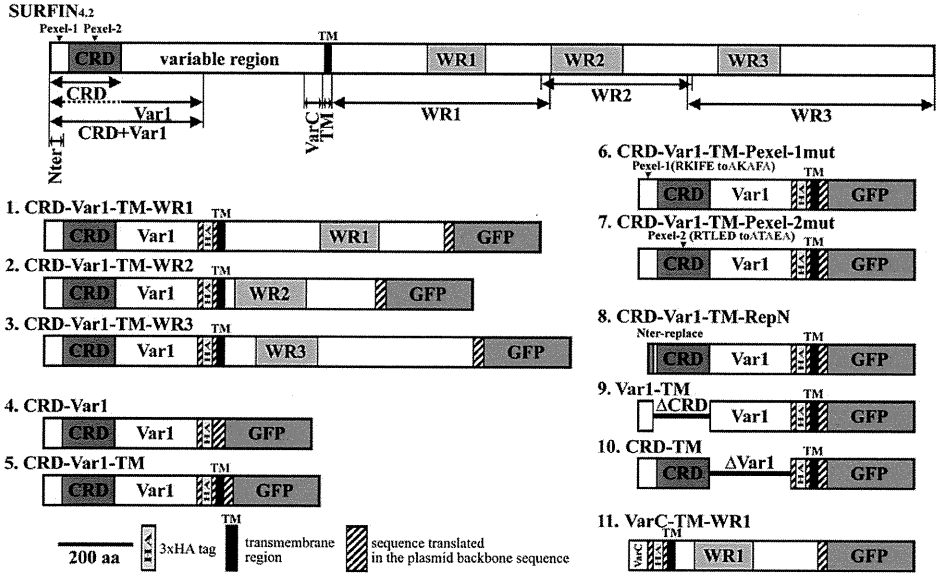

Fig. 1. Schematic structure of the recombinant proteins expressed in the transfected *P. falciparum* lines. CRD, cysteine-rich domain; VarC, C-terminal of the variable region; HA, triple hemagglutinin-tag; Nter, N-terminal; TM, transmembrane; Var1, variable region 1; and WR, tryptophan-rich. ΔCRD or ΔVar1 indicates that CRD or Var1 was deleted from the protein.

were usually detected before the 30th day of culture in the presence of the drug and were subsequently maintained in culture containing 25 nM WR99210.

2.3. Fluorescence live imaging and indirect immunofluorescence assay (IFA)

For fluorescence live imaging, 10 μL of parasite culture were incubated with 1 μg/mL of Hoechst 33342 (Moleculer Probe) for 30 min at 37 °C and placed on a glass slide for observation. Parasites expressing GFPm2 were visualized using a fluorescence microscope (Eclipse 80i; Nikon, Japan) and a digital camera (VB-7010; Keyence, Japan) equipped with 100× oil immersion lens. For IFA, thin smears of *P. falciparum* iRBCs were prepared on glass slides, fixed with 4% paraformaldehyde/0.075% glutaraldehyde in PBS at room temperature for 5 min, rinsed with 50 mM glycine in PBS, and blocked with PBS containing 3% BSA (SIGMA) for 30 min [32]. For single staining, the smears were reacted with rabbit anti-GFP polyclonal antibody (ab6556; Abcam, Cambridge, UK), followed by Alexa-Fluor 488-conjugated secondary anti-rabbit IgG antibody (Invitrogen). For double staining, rabbit anti-GFP antibody and rabbit anti-SBP1 antibody (a kind gift from Dr. T. Tsuboi) were labeled with Alexa-Fluor 488 and-594, respectively, using Zenon® Rabbit IgG labeling kit (Invitrogen). The smears were then incubated with rabbit anti-GFP antibody (1:500) and rabbit anti-SBP1 antiserum (1:1000) in PBS containing 3% BSA for 1 h at 37 °C. Parasite nuclear staining was carried out by adding 4′, 6-diamidino-2-phenylindole (DAPI; Invitrogen; final 1 μg/mL). Stained parasites were mounted with ProLong® Gold antifade reagent (Invitrogen) and visualized as described above. Some images were analyzed by using ImageJ software (1.44p; http://rsbweb.nih.gov/ij/).

2.4. Extraction of parasite proteins and Western blot analysis

Mature trophozoite and schizonts-iRBCs were collected by centrifugation on a 40/70% Percoll–sorbitol gradient. The enriched parasite fractions ($2–4\times10^8$ parasites) were subjected to protein extraction during which process the water-soluble fraction was collected following a freeze–thaw procedure in PBS containing a mixture of protease inhibitors (PI; cOmplete; Roche, Basel, Switzerland) repeated three times. The pellets were washed twice with PBS-PI, and proteins further extracted in PBS-PI containing 1% Triton X-100 (Tx; Calbiochem) for 30 min on ice. The insoluble materials were washed twice with PBS-PI-Tx, then proteins were further extracted by incubation with PBS-PI containing 2% SDS (Nacalai, Japan) for 30 min at room temperature.

Parasite extracts were subjected to electrophoresis on 5–20% SDS-polyacrylamide gradient mini gels (ATTO, Japan) under reducing conditions. The protein bands were transferred from gels to PVDF membranes (Millipore, Billerica, MA). The membranes were then probed with rabbit anti-GFP polyclonal antibody (1:500; ab6556; Abcam), for 1 h at room temperature followed by a secondary incubation with the horseradish peroxidase-conjugated goat anti-rabbit IgG antibodies (Promega) at a concentration of 1:25,000. Purified mouse anti-glycophorin A antibody (CD235a; BD Pharmingen) was used to detect glycophorin A as a positive control. Bands were visualized with Immobilon™ Western Chemiluminescent HRP Substrate (Millipore) and detected using a chemiluminescence detection system (LAS-4000EPUVmini; Fujifilm, Japan). The relative molecular sizes of the proteins were calculated based in reference to the molecular size standards (Precision Plus Dual Color Standards; Bio-Rad).

3. Results

3.1. Successful generation of mini-SURFIN$_{4.2}$ proteins

The production of *P. falciparum* transfectants expressing very large proteins such as SURFIN$_{4.2}$ (predicted molecular weight of 286 kDa in 3D7 parasite line) is technically challenging. Therefore, in order to investigate which region is responsible for the trafficking of SURFIN$_{4.2}$ into the iRBCs, and thence Maurer's clefts, we first attempted to generate and evaluate mini-SURFIN$_{4.2}$ proteins containing regions that are conserved among SURFIN members; N-terminal 419 amino acids containing N-terminal segment (aa 1–50) and CRD (aa 51–195), which is conserved among *P. falciparum* SURFIN members, and the N-terminal side of the variable region (Var1; aa 196–419), which is relatively conserved between SURFIN$_{4.2}$ and SURFIN$_{4.1}$ (identity 19.5% and similarity 28.7%), TM, and either one of the WR domains (WR1,

WR2, or WR3). All mini-SURFIN$_{4.2}$ proteins, SURFIN$_{4.2}$CRD-Var1-TM-WR1, -WR2, or -WR3, were tagged with GFP for visualization (Fig. 1). Although the extracellular region was tagged with triple HA, anti-HA mouse monoclonal antibody (4B2; Wako, Japan) could not detect any signals by IFA and Western blot analysis with unknown reason, thus HA tag was not used in this study. Live imaging using a fluorescence microscope produced only very weak fluorescent signals, and so the precise location of the GFPm2-tagged protein was impossible to assess. By double staining IFA, all mini-SURFIN$_{4.2}$ proteins were observed in the iRBC cytoplasm as punctate dots that co-localized with the Maurer's cleft protein SBP1 [18], indicating that all 3 mini-SURFIN$_{4.2}$ proteins were transported to the Maurer's clefts (Fig. 2). In addition to the Maurer's cleft localized signal, diffuse fluorescence was also observed in the parasite, as well as in the iRBC. As all of the mini-SURFIN$_{4.2}$ proteins were able to traverse the PVM and reach the iRBC cytosol and the Maurer's clefts, we selected SURFIN$_{4.2}$CRD-Var1-TM-WR1 for further evaluation.

3.2. The TM region, but not the WR domain is essential for the SURFIN$_{4.2}$ trafficking to the iRBC and Maurer's clefts

In order to evaluate the importance of the TM region and WR domain in SURFIN$_{4.2}$ trafficking, we generated parasites expressing only SURFIN$_{4.2}$CRD-Var1 (TM and WR were removed) or SURFIN$_{4.2}$ CRD-Var1-TM (WR was removed). By live imaging, weak, but detectable GFP signals were observed for these transfectants, and we found that SURFIN$_{4.2}$CRD-Var1 was exclusively located in the parasite cytoplasm, as would be expected for a protein lacking a signal sequence for transport to the ER. We speculate that the protein was located within the parasite cytosol (Fig. 3A). In contrast, SURFIN$_{4.2}$ CRD-Var1-TM was observed in a punctate dot pattern in the iRBC, in addition to diffuse fluorescence in the parasite cytoplasm. By double staining IFA, SURFIN$_{4.2}$CRD-Var1 was observed only in the parasite, confirming the live imaging results, whereas SURFIN$_{4.2}$CRD-Var1-TM colocalized with SBP1, indicating a Maurer's cleft localization (Fig. 3B). Thus, the IFA data indicate that the SURFIN$_{4.2}$ cytoplasmic region containing WR domain is not required for trafficking to the iRBC or Maurer's clefts, but the TM region is essential.

A diffused fluorescence pattern in the iRBC, as observed for the mini-SURFIN$_{4.2}$ proteins, appeared to be reduced for SURFIN$_{4.2}$CRD-Var1-TM with the double staining IFA images. Because the single staining with Alexa-Fluor 488-conjugated secondary antibody gave clearer images than the double staining using the Zenon antibody-labeling kit, we used two representative single staining images to measure and compare the signal intensity of the recombinant proteins in the iRBC cytosol for SURFIN$_{4.2}$CRD-Var1-TM and SURFIN$_{4.2}$CRD-Var1-TM-WR1. After subtracting background signals, signal intensities in the iRBC cytosol for SURFIN$_{4.2}$CRD-Var1-TM were 13 to 22 units (Fig. 4B; CRD-Var1-TM #1 and #2), whereas those for SURFIN$_{4.2}$CRD-Var1-TM-WR were 66 and 69 units (Fig. 4B; CRD-Var1-TM-WR1 #1 and #2, respectively). This indicates that the fluorescence signal in the iRBC cytosol is weaker for SURFIN$_{4.2}$CRD-Var1-TM than SURFIN$_{4.2}$ CRD-Var1-TM-WR1 and suggests that the SURFIN$_{4.2}$CRD-Var1-TM is less abundant in iRBC cytosol than SURFIN$_{4.2}$CRD-Var1-TM-WR1.

In order to evaluate their solubility, parasite proteins were sequentially extracted by a repeated-freeze thaw procedure (FT; water-soluble fraction protein), followed by Tx extraction (Tx; membrane bound protein), and SDS extraction (SDS; Tx-insoluble fraction) and were detected with rabbit anti-GFP antibody. About 105-kDa bands were detected for SURFIN$_{4.2}$CRD-Var1 and SURFIN$_{4.2}$CRD-Var1-TM and a 230-kDa band for SURFIN$_{4.2}$CRD-Var1-TM-WR1 by Western blot. Expected band sizes were 83, 86, and 158 kDa, respectively (Fig. 5A). Although the band sizes detected by Western blot are much larger than the expected size, this is not an uncommon observation for *P. falciparum*-derived proteins which have a deviated amino acid composition due to a highly A/T-rich genome (76.3% in the exon) [33]. In addition to the target protein bands, a ~60-kDa band was observed for all fractions (Fig. 5A), but this band was also observed in the extract from the wild-type non-transfected MS822 parasite, and so was not derived from the recombinant proteins expressed in the transfected parasite lines. Although the identity of this band is unclear, it is likely derived from parasites, because this band was not

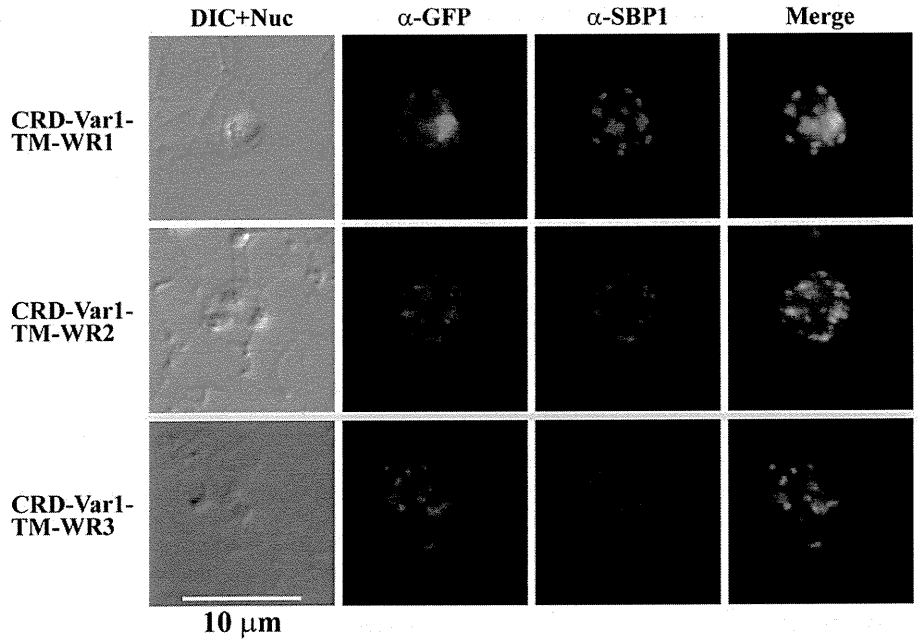

Fig. 2. Indirect immunofluorescence assay of three mini-SURFIN$_{4.2}$ proteins. Double staining IFA for 3 mini-SURFIN$_{4.2}$-expressing transfectants is shown. α-GFP and α-SBP1 indicate anti-GFP (mini-SURFIN$_{4.2}$) and anti-SBP1 (Maurer's cleft protein). Negative controls using normal rabbit antibody did not produce detectable signals (not shown). CRD, cysteine-rich domain; TM, transmembrane; Var1, variable region 1; and WR, tryptophan-rich.

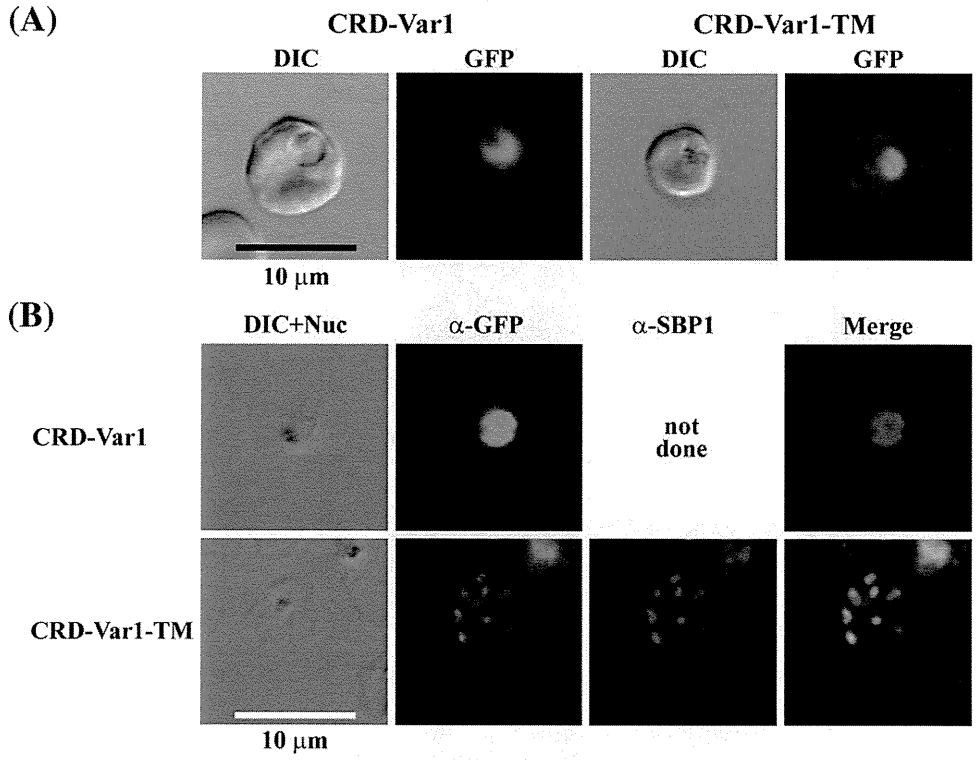

Fig. 3. Indirect immunofluorescence assay of $SURFIN_{4.2}$CRD-Var1 and $SURFIN_{4.2}$CRD-Var1-TM proteins. (A) Live imaging of GFP-expressing parasites. (B) Single staining for $SURFIN_{4.2}$CRD-Var1 and double staining for $SURFIN_{4.2}$CRD-Var1-TM with anti-GFP (α-GFP, green) and anti-SBP1 (α-SBP1, red). Nuclei were stained with DAPI. Negative control using normal rabbit antibody did not produce detectable signals (not shown). CRD, cysteine-rich domain; TM, transmembrane; and Var1, variable region 1.

observed in the extract from the parasite-uninfected RBC (Fig. 5B). Positive glycophorin A bands for the extracts from both the wild-type parasite and the uninfected RBC indicated that the protein extraction from the uninfected RBC was successful. It should be noted that the rabbit anti-GFP antibodies did not show any signal when wild-type parasites were subjected to IFA. We found that $SURFIN_{4.2}$CRD-Var1 was exclusively detected in the soluble FT fraction, indicating that this protein was in soluble form, which is consistent with the observation of its localization in the parasite's cytoplasm (Fig. 3). $SURFIN_{4.2}$CRD-Var1-TM was detected in the Tx-soluble fraction more abundantly than in the Tx-insoluble SDS fraction. Conversely, $SURFIN_{4.2}$CRD-Var1-TM-WR1 was detected in the SDS fraction more abundantly than in the Tx fraction. Thus both proteins appeared to be associated with membrane structures, and the cytoplasmic region containing the WR1 may be responsible for their difference in solubility.

3.3. $SURFIN_{4.2}$ is trafficked to the iRBC cytosol in a PEXEL-independent manner

$SURFIN_{4.2}$ contains two PEXEL-like sequences, one was termed Pexel 1 in this study and was located at the N-terminal region, spanning aa 25–29 (R_KI_FE), for which the 3rd position was isoleucine instead of leucine in the authentic PEXEL motif. The other was termed Pexel 2, and was located in the CRD at aa 118–122 (R_TL_ED). In order to evaluate their involvement in the transport of the protein into the iRBC, we generated two parasite lines expressing $SURF_{4.2}$CRD-Var1-TM-Pexel-1mut or $SURF_{4.2}$CRD-Var1-TM-Pexel-2mut, for which the conserved residues of the PEXEL-like sequence were replaced by alanine (A_KA_FA or A_TA_EA, respectively). Double staining IFA revealed that $SURFIN_{4.2}$CRD-Var1-TM-Pexel-1mut and -2mut both showed a punctate dot pattern in the iRBC that colocalized with the Maurer's cleft protein SBP1 along with parasite localized fluorescence (Fig. 6A). Thus, there was no appreciable difference between the trafficking of these proteins and that of the original $SURFIN_{4.2}$CRD-Var1-TM recombinant protein. These observations suggest that the PEXEL-like sequences of $SURFIN_{4.2}$ play no evident function in the transport of $SURFIN_{4.2}$ to the iRBC cytosol and Maurer's clefts. Thus, $SURFIN_{4.2}$ is being trafficked as a PNEP.

3.4. Removal of N-terminal 42 amino acid segment, CRD, or Var1 did not prevent the $SURFIN_{4.2}$ trafficking to the iRBC cytosol and Maurer's clefts

To further evaluate the importance of the different regions of the $SURFIN_{4.2}$ extracellular region in the trafficking of the protein to the iRBC, we generated three following parasite lines: two lines expressing $SURFIN_{4.2}$Var1-TM or $SURFIN_{4.2}$CRD-TM, in which the CRD or Var1 region were deleted from $SURFIN_{4.2}$CRD-Var1-TM and the one line expressing $SURFIN_{4.2}$CRD-Var1-TM-RepN, in which the N-terminal first 42 amino acids of $SURFIN_{4.2}$CRD-Var1-TM was replaced by the N-terminal first 15 amino acids of *P. falciparum* adenylosuccinate lyase (*Pf*ASL), an enzyme involved in the purine metabolism in the cell cytosol and is not considered to be transported to the iRBC [34]. Double staining IFA revealed that $SURFIN_{4.2}$Var1-TM and $SURFIN_{4.2}$CRD-TM colocalized with SBP1 in a punctate dot pattern in the iRBC and was also present in the parasite cytoplasm. No difference was observed between these two lines and the line expressing $SURFIN_{4.2}$CRD-Var1-TM (Fig. 6B). A more diffused iRBC localization with less obvious dot pattern formation was observed with the line expressing $SURF_{4.2}$CRD-Var1-TM-RepN compared to that expressing $SURFIN_{4.2}$CRD-Var1-TM. Nonetheless, the transport of the $SURF_{4.2}$

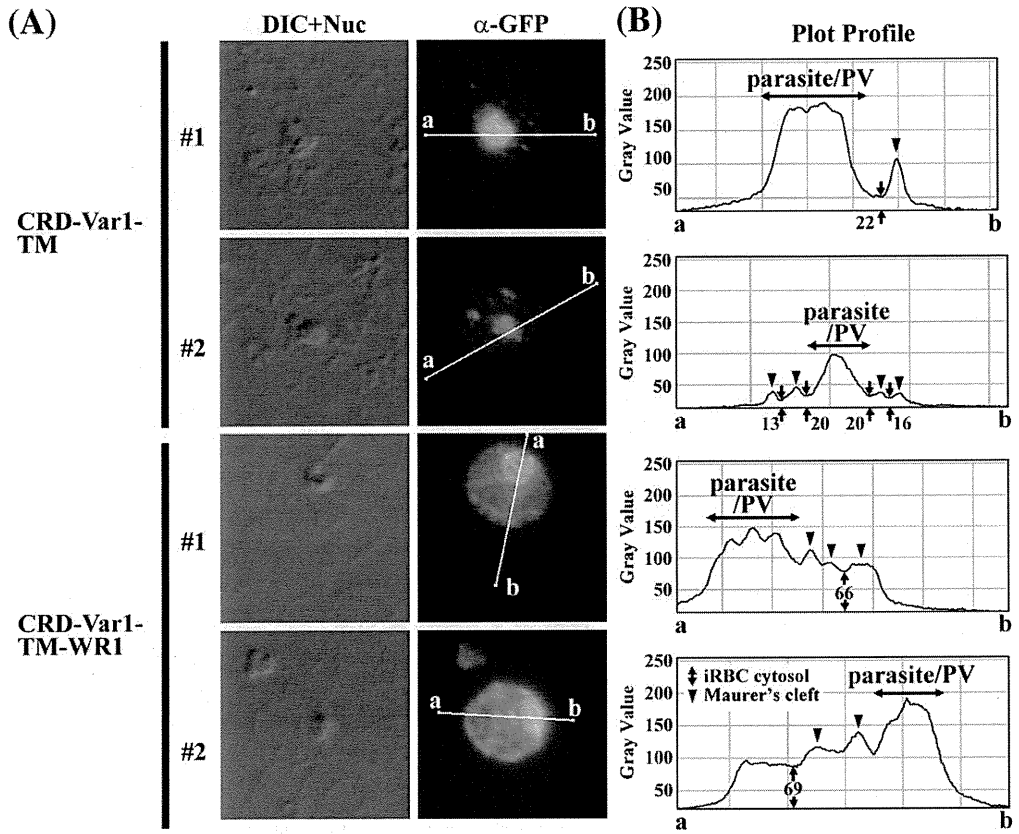

Fig. 4. Comparison of the signal intensity between SURFIN$_{4.2}$CRD-Var1-TM and SURFIN$_{4.2}$CRD-Var1-TM-WR1 proteins in the parasite-infected red blood cell. (A) Indirect immunofluorescence assay with anti-GFP antibody was performed for both parasites expressing SURFIN$_{4.2}$CRD-Var1-TM and SURFIN$_{4.2}$CRD-Var1-TM-WR1 at the same time. The fluorescence signal intensities were measured from point (a) to (b). (B) Plot profiles were made by using ImageJ software for the regions shown in panel A. Parasite/PV indicates parasite cytosol or parasitophorous vacuole. Signal intensities are shown by gray level pixel intensity values.

CRD-Var1-TM-RepN protein was not completely abrogated and signals, although faint, still colocalized with the Maurer's cleft SBP1. Thus, any of the N-terminal segment (aa 1–42), the CRD (aa 46–196), or the variable region (aa 198–733) at the extracellular region of SURFIN$_{4.2}$ do not carry a specific motif necessary for protein transport to the iRBC.

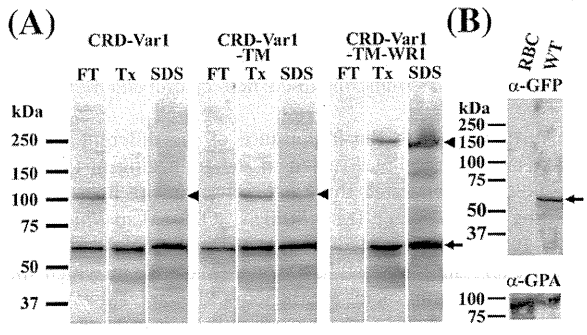

Fig. 5. Western blot of SURFIN$_{4.2}$CRD, SURFIN$_{4.2}$CRD-TM, and SURFIN$_{4.2}$CRD-TM-WR1 proteins subjected to different extraction procedures. (A) Parasite proteins were sequentially extracted by repeated-freeze thaw procedure (FT; soluble fraction protein), followed by Triton X-100 extraction (Tx; membrane bound protein), and SDS extraction (SDS, Tx-insoluble fraction) and detected with rabbit anti-GFP antibody. (B) Triton X-100 extracts of parasite-uninfected red blood cell (RBC) and the wild-type MS822 parasite line (WT) were subjected for Western blot analysis with rabbit anti-GFP (α-GFP) or mouse anti-glycophorin A (α-GPA). The arrow marks a ~60-kDa band also observed in wild-type parasites, but not in uninfected RBC. Arrowheads indicate expressed recombinant proteins, SURFIN$_{4.2}$CRD, SURFIN$_{4.2}$CRD-TM, and SURFIN$_{4.2}$CRD-TM-WR1.

To confirm these findings, we truncated the entire external domain from the mini-SURFIN$_{4.2}$ protein, and added 50 amino acids (SSGQVRRSGGQGSETYIVGTSQSGFHKNEVIPSIKDKSGKTQIVSNEKGG) preceding the TM region in order to support the integrality of the TM region for membrane insertion, to generate a parasite expressing SURFIN$_{4.2}$VarC-TM-WR1, thus this protein contains 50 amino acids derived from SURFIN$_{4.2}$ followed by a triple HA tag as an extracellular region. The recombinant protein was transported to the iRBC and observed in a punctate dot pattern in the iRBC cytosol, colocalizing with SBP1 (Fig. 7). This indicates that the extracellular region of SURFIN$_{4.2}$ is not required for the trafficking of the protein to the iRBC.

4. Discussion

In this study, we generated GFPm2-fused mini-SURFIN$_{4.2}$ proteins that, following their transfection into a *P. falciparum* parasite line, was observed to be trafficked into the iRBC and Maurer's clefts. Using this system, we then attempted to identify the specific region of the protein responsible for the iRBC and/or Maurer's cleft localization. We found that the TM region, but not the cytoplasmic region containing WR domain was essential for protein transport. We consider it likely that the TM region is responsible for initiating the trafficking of the protein into the ER. Two PEXEL-like sequences were found not to be essential for the movement of the protein into the iRBC and Maurer's clefts, indicating that SURFIN$_{4.2}$ trafficking is PEXEL-independent. N-terminal replacement, deletion of the CRD or Var region did not

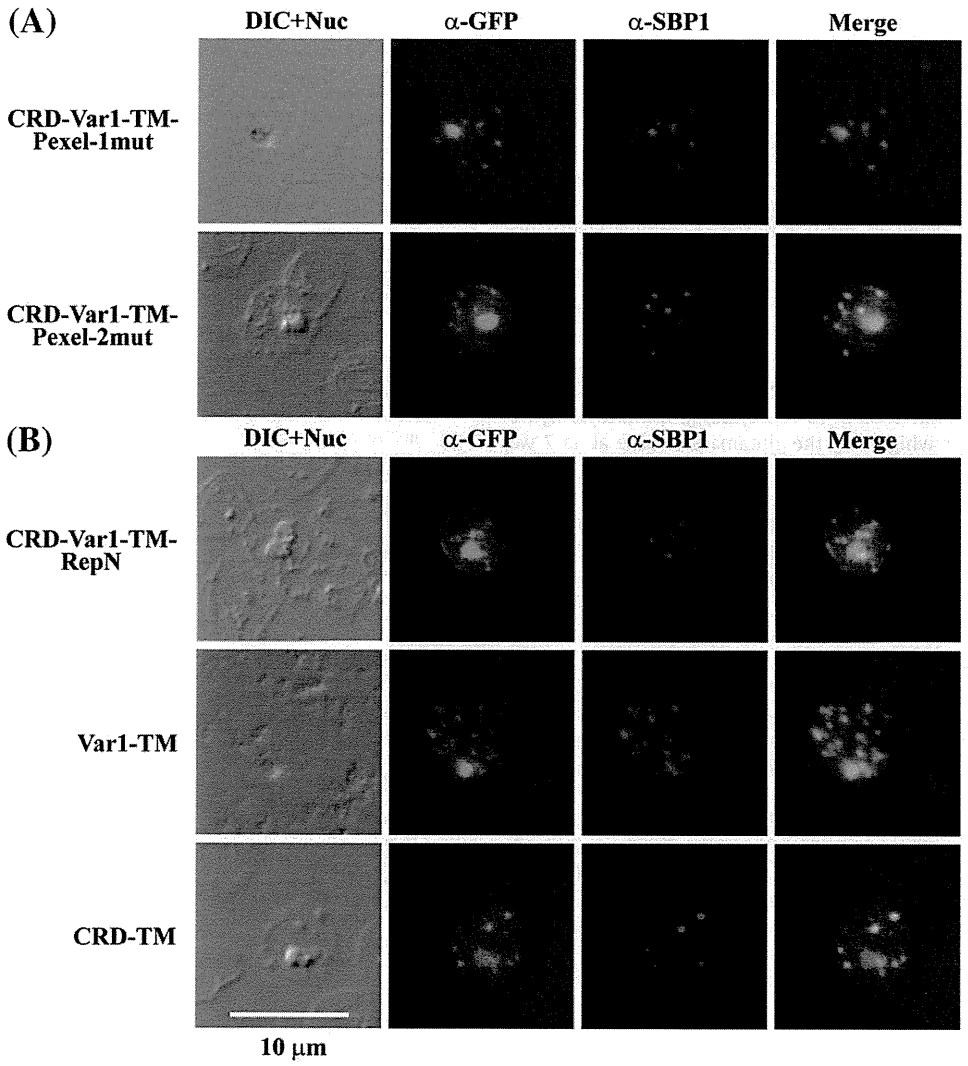

Fig. 6. Indirect immunofluorescence assay of modified SURFIN$_{4.2}$CRD-Var1-TM proteins. (A) Double staining for SURFIN$_{4.2}$CRD-Var1-TM-Pexel-1mut and CRD-Var1-TM-Pexel-2mut, and for (B) CRD-Var1-TM-RepN, Var1-TM, and CRD-TM proteins with anti-GFP (α-GFP, green) and anti-SBP1 (α-SBP1, red). Nuclei were stained with DAPI. Negative control using normal rabbit antibody did not produce detectable signals (not shown). CRD, cysteine-rich domain; RepN, N-terminus replacement; TM, transmembrane; and Var1, variable region 1.

prevent iRBC and Maurer's cleft localization, suggesting that no trafficking motif exists in these regions.

By sequential extraction of recombinant SURFIN$_{4.2}$ proteins, we found that mini-SURFIN$_{4.2}$ with an intact WR domain showed more resistance to Triton-X 100 extraction than a similar protein in which WR domain had been removed. As endogenous SURFIN$_{4.2}$ was insoluble in Triton-X 100 but soluble in SDS [26], we suggest that the cytoplasmic region, probably the WR domain, contributes to this difference. Insolubility with a neutral detergent such as Triton-X 100, was also reported for *Pf*EMP1 [35]. A large degree of sequence similarity was shown between the cytoplasmic WR domain of SURFIN$_{4.2}$, *Pf*EMP1, and another iRBC protein *Pf*332 [26]. The cytoplasmic regions of both *Pf*EMP1 and *Pf*332 are known to bind to RBC actin, the former also binding to spectrin [36,37]. Therefore, we

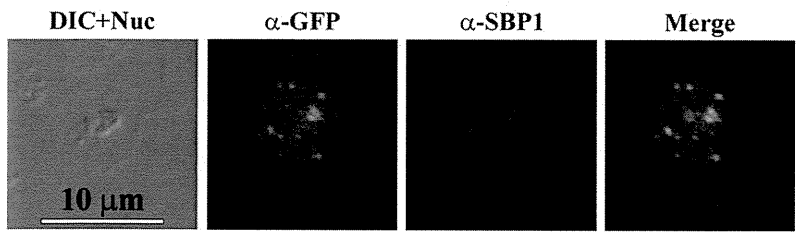

Fig. 7. Indirect immunofluorescence assay of SURFIN$_{4.2}$VarC-TM-WR1 protein. Double staining with anti-GFP (α-GFP, green) and anti-SBP1 (α-SBP1, red). Nuclei were stained with DAPI. Negative control using normal rabbit antibody did not produce detectable signals (not shown).

suggest that the WR domain of SURFIN$_{4.2}$ also associates with the RBC cytoskeleton, although further evaluation is required to assess this hypothesis.

Similar to most of the PNEPs reported so far, the SURFIN$_{4.2}$ TM region was found to be essential for protein trafficking. *Pf*SBP1 [11], MAHRP1 [19] and REX2 [24] share this feature, with their TM regions known to play important roles in protein transport. However, the N-terminal sequence of these PNEPs was also found to be essential for correct protein trafficking. In addition to the TM region, *Pf*SBP1 was shown to require the N-terminal segment at aa 16–26, which contain highly negative net charge residues (DEPTQLQDAVP) for transport into the iRBC [11]. This may also be the case for MAHRP1, as the N-terminal 50 amino acids of this protein, which is acidic, along with *Pf*SBP1 TM region is able to transport protein into the iRBC [11]. Conversely, REX2 appears to contain region resembling a PEXEL motif after cleavage in the ER at aa 5–10 ($L_5xE_7hhS_{10}$; h indicates hydrophobic residues), for which only the glutamate residue at aa 7 was found to be critical for trafficking [24]. In the mini-SURFIN$_{4.2}$ proteins we expressed in this study, none of the regions from the SURFIN$_{4.2}$ extracellular regions shown to be indispensable for trafficking to the iRBC, thus the trafficking of SURFIN$_{4.2}$ appears not depend on specific sorting signals, nor potential escorter proteins, but other factors in addition to the TM region.

Acknowledgments

We thank R. Culleton for critical reading and helpful comments. We are grateful to G. McFadden for *Pf*CRT 5′-pENTR4/1, GFP-pENTR2/3, and pCHDR-3/4, D. Jacobus for WR99210, T. Tsuboi for anti-*Pf*SBP1 rabbit serum, N. Iyoku for her expertise, and I. Sekine, head of the Nagasaki Red Cross Blood Center for human RBC and plasma. This work was supported in part by Grants-in-Aids for Scientific Research 20406009 and the Global COE Program, Nagasaki University, from the Ministry of Education, Culture, Sports, Science and Technology (MEXT) of Japan, and Daiichi-Sankyo Foundation of Life Science (to O.K.). J.A. is a recipient of MEXT PhD scholarship, Japan. All experiments conducted in this study were approved by the committee for Living Modified Organisms in Nagasaki University.

Appendix A. Supplementary data

Supplementary data to this article can be found online at doi:10.1016/j.parint.2011.05.003.

References

[1] Tilley L, Sougrat R, Lithgow T, Hanssen E. The twists and turns of Maurer's cleft trafficking in *P. falciparum*-infected erythrocytes. Traffic 2008;9:187–97.
[2] Przyborski JM, Wickert H, Krohne G, Lanzer M. Maurer's clefts — a novel secretory organelle? Mol Biochem Parasitol 2003;132:17–26.
[3] Lanzer M, Wickert H, Krohne G, Vincensini L, Braun-Breton C. Maurer's clefts: a novel multi-functional organelle in the cytoplasm of *Plasmodium falciparum*-infected erythrocytes. Int J Parasitol 2006;36:23–36.
[4] Wickham ME, Rug M, Ralph SA, Klonis N, McFadden GI, Tilley L, et al. Trafficking and assembly of the cytoadherence complex in *Plasmodium falciparum*-infected human erythrocytes. EMBO J 2001;20:5636–49.
[5] Baruch DI. Adhesive receptors on malaria-parasitized red cells. Baillière's Best Pract Res Clin Haematol 1999;12:747–61.
[6] Chen Q, Schlichtherle M, Wahlgren M. Molecular aspects of severe malaria. Clin Microbiol Rev 2000;13:439–50.
[7] Newbold C, Craig A, Kyes S, Rowe A, Fernandez-Reyes D, Fagan T. Cytoadherence, pathogenesis and the infected red cell surface in *Plasmodium falciparum*. Int J Parasitol 1999;29:927–37.
[8] Hiller NL, Bhattacharjee S, van Ooij C, Liolios K, Harrison T, Lopez-Estraño C, et al. A host-targeting signal in virulence proteins reveals a secretome in malarial infection. Science 2004;306:1934–7.
[9] Marti M, Good RT, Rug M, Knuepfer E, Cowman AF. Targeting malaria virulence and remodeling proteins to the host erythrocyte. Science 2004;306:1930–3.
[10] Marti M, Baum J, Rug M, Tilley L, Cowman AF. Signal-mediated export of proteins from the malaria parasite to the host erythrocyte. J Cell Biol 2005;171:587–92.
[11] Saridaki T, Fröhlich KS, Braun-Breton C, Lanzer M. Export of *Pf*SBP1 to the *Plasmodium falciparum* Maurer's clefts. Traffic 2009;10:137–52.
[12] Boddey JA, Hodder AN, Günther S, Gilson PR, Patsiouras H, Kapp EA, et al. An aspartyl protease directs malaria effector proteins to the host cell. Nature 2010;463:627–31.
[13] Russo I, Babbitt S, Muralidharan V, Butler T, Oksman A, Goldberg DE. Plasmepsin V licenses *Plasmodium* proteins for export into the host erythrocyte. Nature 2010;463:632–6.
[14] de Koning-Ward TF, Gilson PR, Boddey JA, Rug M, Smith BJ, Papenfuss AT, et al. A newly discovered protein export machine in malaria parasites. Nature 2009;459:945–9.
[15] Melcher M, Muhle RA, Henrich PP, Kraemer SM, Avril M, Vigan-Womas I, et al. Identification of a role for the *Pf*EMP1 semi-conserved head structure in protein trafficking to the surface of *Plasmodium falciparum* infected red blood cells. Cell Microbiol 2010;12:1446–62.
[16] van Ooij C, Tamez P, Bhattacharjee S, Hiller NL, Harrison T, Liolios K, et al. The malaria secretome: from algorithms to essential function in blood stage infection. PLoS Pathog 2008;4:e1000084.
[17] Spielmann T, Hawthorne PL, Dixon MW, Hannemann M, Klotz K, Kemp DJ, et al. A cluster of ring stage-specific genes linked to a locus implicated in cytoadherence in *Plasmodium falciparum* codes for PEXEL-negative and PEXEL-positive proteins exported into the host cell. Mol Biol Cell 2006;17:3613–24.
[18] Blisnick T, Morales Betoulle ME, Barale JC, Uzureau P, Berry L, Desroses S, et al. *Pf*sbp1, a Maurer's cleft *Plasmodium falciparum* protein, is associated with the erythrocyte skeleton. Mol Biochem Parasitol 2000;111:107–21.
[19] Spycher C, Klonis N, Spielmann T, Kump E, Steiger S, Tilley L, et al. MAHRP-1, a novel *Plasmodium falciparum* histidine-rich protein, binds ferriprotoporphyrin IX and localizes to the Maurer's clefts. J Biol Chem 2003;278:35373–83.
[20] Hawthorne PL, Trenholme KR, Skinner-Adams TS, Spielmann T, Fischer K, Dixon MW, et al. A novel *Plasmodium falciparum* ring stage protein, REX, is located in Maurer's clefts. Mol Biochem Parasitol 2004;136:181–9.
[21] Hanssen E, Hawthorne P, Dixon MW, Trenholme KR, McMillan PJ, Spielmann T, et al. Targeted mutagenesis of the ring-exported protein-1 of *Plasmodium falciparum* disrupts the architecture of Maurer's cleft organelles. Mol Microbiol 2008;69:938–53.
[22] Saridaki T, Sánchez CP, Pfahler J, Lanzer M. A conditional export system provides new insights into protein export in *Plasmodium falciparum*-infected erythrocytes. Cell Microbiol 2008;10:2483–95.
[23] Spielmann T, Gilberger TW. Protein export in malaria parasites: do multiple export motifs add up to multiple export pathways? Trends Parasitol 2009;26:6–10.
[24] Haase S, Herrmann S, Grüring C, Heiber A, Jansen PW, Langer C, et al. Sequence requirements for the export of the *Plasmodium falciparum* Maurer's clefts protein REX2. Mol Microbiol 2009;71:1003–17.
[25] Dixon MW, Hawthorne PL, Spielmann T, Anderson KL, Trenholme KR, Gardiner DL. Targeting of the ring exported protein 1 to the Maurer's clefts is mediated by a two-phase process. Traffic 2008;9:1316–26.
[26] Winter G, Kawai S, Haeggström M, Kaneko O, von Euler A, Kawazu S, et al. SURFIN is a polymorphic antigen expressed on *Plasmodium falciparum* merozoites and infected erythrocytes. J Exp Med 2005;201:1853–63.
[27] van Dooren GG, Marti M, Tonkin CJ, Stimmler LM, Cowman AF, McFadden GI. Development of the endoplasmic reticulum, mitochondrion and apicoplast during the asexual life cycle of *Plasmodium falciparum*. Mol Microbiol 2005;57:405–19.
[28] Le Roch KG, Zhou Y, Blair PL, Grainger M, Moch JK, Haynes JD, et al. Discovery of gene function by expression profiling of the malaria parasite life cycle. Science 2003;301:1503–8.
[29] Aurrecoechea C, Brestelli J, Brunk BP, Dommer J, Fischer S, Gajria B, et al. PlasmoDB: a functional genomic database for malaria parasites. Nucleic Acids Res 2009;37:D539–43.
[30] Nakazawa S, Culleton R, Maeno Y. In vivo and in vitro gametocyte production of *Plasmodium falciparum* isolates from Northern Thailand. Int J Parasitol 2011;41:317–23.
[31] Deitsch K, Driskill C, Wellems T. Transformation of malaria parasites by the spontaneous uptake and expression of DNA from human erythrocytes. Nucleic Acids Res 2001;29:850–3.
[32] Tonkin CJ, van Dooren GG, Spurck TP, Struck NS, Good RT, Handman E, et al. Localization of organellar proteins in *Plasmodium falciparum* using a novel set of transfection vectors and a new immunofluorescence fixation method. Mol Biochem Parasitol 2004;137:13–21.
[33] Gardner MJ, Hall N, Fung E, White O, Berriman M, Hyman RW, et al. Genome sequence of the human malaria parasite *Plasmodium falciparum*. Nature 2002;419:498–511.
[34] Marshall VM, Coppel RL. Characterisation of the gene encoding adenylosuccinate lyase of *Plasmodium falciparum*. Mol Biochem Parasitol 1997;88:237–41.
[35] Aley SB, Sherwood JA, Howard RJ. Knob-positive and knob-negative *Plasmodium falciparum* differ in expression of a strain-specific malarial antigen on the surface of infected erythrocytes. J Exp Med 1984;160:1585–90.
[36] Oh SS, Voigt S, Fisher D, Yi SJ, LeRoy PJ, Derick LH, et al. *Plasmodium falciparum* erythrocyte membrane protein 1 is anchored to the actin-spectrin junction and knob-associated histidine-rich protein in the erythrocyte skeleton. Mol Biochem Parasitol 2000;108:237–47.
[37] Waller KL, Stubberfield LM, Dubljevic V, Buckingham DW, Mohandas N, Coppel RL, et al. Interaction of the exported malaria protein *Pf*332 with the red blood cell membrane skeleton. Biochim Biophys Acta 2010;1798:861–71.

Applications of triphenylpyrylium salt-sensitized electron transfer photo-oxygenation reactions to the synthesis of benzo-fused 1,4-diaryl-2,3-dioxabicyclo[2.2.2]octanes as new antimalarial cyclic peroxides

Masaki Kamata,[1*] Jun-ichi Hagiwara,[1] Tomoko Hokari,[1] Chiharu Suzuki,[1] Ryohta Fujino,[1] Sayaka Kobayashi,[1] Hye-Sook Kim,[2] Yusuke Wataya[2]

Abstract Benzo-fused 1,4-diaryl-2,3-dioxabicyclo[2.2.2]octanes **4a-d** (**4a**: Ar = C_6H_5, **4b**: Ar = *p*-FC_6H_4, **4c**: Ar = *p*-MeC_6H_4, **4d**: Ar = *p*-$MeOC_6H_4$) were synthesized by utilizing 2,4,6-triphenylpyrylium tetrafluoroborate ($TPPBF_4$)-sensitized photoinduced electron transfer (PET)-promoted oxygenation reactions and their in vitro antimalarial activities were evaluated. The results show that these substances have sufficiently high activities to enable them to serve as antimalarial lead compounds. In addition, $TPPBF_4$–biphenyl-cosensitized PET oxygenation process was demonstrated to serve as an efficient method for introduction of an O–O moiety in the construction of antimalarial cyclic peroxides.

Keywords Photoinduced electron transfer · Single electron transfer · Photo-oxygenation · Triphenylpyrylium salt · Cyclic peroxide · Antimalarial activity

---

[1] M. Kamata, J. Hagiwara, T. Hokari, C. Suzuki, R. Fujino, S. Kobayashi
Department of Chemistry, Faculty of Education, Niigata University, Ikarashi, Niigata 950-2181, Japan
e-mail: kamata@ed.niigata-u.ac.jp

[2] H.-S. Kim, Y. Wataya
Division of International Infectious Diseases Control, Faculty of Pharmaceutical Sciences, Graduate School of Medicine, Dentistry and Pharmaceutical Sciences, Okayama University, Tsushima Naka 1–1–1 Kita-Ku, Okayama City, Okayama 700-8530, Japan
e-mail: hskim@cc.okayama-u.ac.jp

Introduction

Owing to the fact that malaria parasites rapidly develop resistance to antimalarial alkaloids, such as chloroquine and mefloquine, the discovery that non-alkaloidal endoperoxides such as artemisinin and related compounds serve as antimarial agents stimulated a number of synthetic and mechanistic studies [1–9]. In particular, a considerable effort has been devoted to the preparation and evaluation of structurally simple, more potent antimalarial cyclic peroxides. Posner reported that 1,4-diaryl-2,3-dioxabicyclo[2.2.2]octanes **1a-b** [10], 1,4-diaryl-2,3-dioxabicyclo[2.2.2]oct-5-enes **2a-c** [10], and 1,5-diaryl-6,7-dioxabicyclo[3.2.2]nonane **3d** [11, 12] are potent antimalarials (Scheme 1). Later, we also described the synthesis, degradation mechanism, and antimalarial activities of endoperoxides **1a-d** [13], **2a-d** [14–16], and **3a-d** [17].

During the course of ongoing investigations of the utilization of single electron transfer (SET)-promoted reactions in synthetic organic chemistry [18–26] and the development of new antimalarial cyclic peroxides [13, 14, and 17], we became interested in benzo-fused 1,4-diaryl-2,3-dioxabicyclo[2.2.2]octane targets **4a-d** possessing a similar framework to **1** and **2**. While it has been reported that **4a** can be synthesized by using 9,10-dicyanoanthracene (DCA)-sensitized PET oxygenation of 1,2-bis(1-phenylethenyl)benzene **5a** through a cyclization and oxygenation process that is similar to that for the preparations of **1** and **3** [27, 28], the yield of the reaction was relatively low (< 50%). In addition, syntheses of other derivatives **4b-d** and an assessment of the antimalarial activities of **4a-d** have not been explored. In an earlier effort, we demonstrated that **3a-c** can be efficiently prepared by using 2,4,6-triphenylpyrylium tetrafluoroborate ($TPPBF_4$) sensitized PET oxygenation of the corresponding 2,6-diaryl-1,6-heptadienes and that these substances can be readily separated by using chromatography as a consequence of the ionic character of $TPPBF_4$ [17]. These observations stimulated our interest in the application of $TPPBF_4$-sensitized PET oxygenation reactions to conversions of 1,2-bis(1-arylethenyl)benzenes **5a-d** to the corresponding bicyclic peroxides **4a-d**. Below, we describe the results of a recent study that has led to concise syntheses of bicyclic peroxides **4a-d**, utilizing $TPPBF_4$-sensitized PET oxygenation reactions, and an evaluation of their antimalarial properties.

(Scheme 1)

Results and discussion

1,2-Bis(1-arylethenyl)benzenes **5a-d** were prepared by using methylation reactions of the corresponding *o*-diaroylbenzenes **6a-d** in THF employing the Tebbe reagent (Scheme 2). The *o*-diaroylbenzenes **6a-d** were prepared via Grignard addition reactions of the corresponding arylmagnesium bromides with phthaloyl chloride in THF [29]. The oxidation potentials of **5a-d** in CH_3CN containing 0.1 M Et_4NClO_4 were determined by using cyclic voltammetry to be +1.49, +1.44, +1.38, and +1.19 V ($E_{1/2}^{ox}$ *vs.* SCE), respectively. The estimated reduction potential of the excited singlet state of $TPPBF_4$ ($^*E_{1/2}^{red}$ *vs.* SCE) is *ca.* +2.50 V [30]. Therefore, the calculated ΔG° values for SET between **5a-d** and the excited singlet state of $TPPBF_4$ in CH_3CN are −25, −26, −27, and −32 kcal mol^{-1}, respectively [22, 30-34]. Similarly the calculated ΔG° values for SET between **5a-d** and the excited singlet state of DCA ($^*E_{1/2}^{red}$ = +1.90 V *vs.* SCE) in CH_3CN are −11, −12, −13, and −18 kcal mol^{-1}, respectively. Consequently, SET from **5a-d** to the excited singlet states of $TPPBF_4$ and DCA are highly exothermic.

(Scheme 2)

PET oxygenation reactions were carried out in dry CH_3CN solutions of **5a-d** (20 mM) and a sensitizer ($TPPBF_4$: 2 mM or DCA: 0.2 mM) with or without biphenyl (Bip: 60 mM) being present. The solutions were irradiated at 20 °C under an oxygen atmosphere using a 2-kW Xe lamp and a Toshiba L-39 filter (> 390 nm). The progress of each reaction was monitored by using thin layer chromatography and further analyzed by utilizing 200 MHz ^{1}H-NMR spectroscopy ($CDCl_3$). The peroxides **4a-d** were isolated by using silica gel chromatography. As the results summarized in Table 1 show, $TPPBF_4$-sensitized PET oxygenation reactions of **5a-d** produce the corresponding bicyclic peroxides **4a-d** in moderate to good yields (60–71%, run 3, 7, 11, and 15) along with small amounts of *o*-diaroylbenzenes **6a-d**, whereas processes promoted by using DCA as a sensitizer are less efficient (36–58%, run 1, 5, 9, and 13) and they generate appreciable amounts of **6a-d**. Based on the earlier observation by Schaap that the use of biphenyl (Bip) as a cosensitizer leads to a dramatic efficiency enhancement of DCA-sensitized PET oxygenation reactions of aryl-substituted oxiranes [26, 35–38], Bip was incorporated in the photo-oxygenation mixture to improve the

yields for formation of **4a-d**. We observed that $TPPBF_4$–Bip-cosensitized PET oxygenation reactions of **5a-d** take place with significantly improved yields (66–88%, run 4, 8, 12, and 16) to form **4a-d** along with diminished production of **6a-d**. Although the yields of **4a-d** are similarly improved when DCA–Bip-cosensitization conditions are employed (44–68%, run 2, 6, 10, and 14), they did not exceed those of the $TPPBF_4$–Bip-cosensitized oxygenation reactions. The combined results indicate that the process utilizing $TPPBF_4$–Bip-cosensitization is the best method to synthesize **4a-d**, and especially **4a-c** which possess relatively weaker electron-donating aromatic groups.

(Table 1)

On the basis of the results of this and related studies [11–17, 22, 26-28, 30, and 39–41], it is possible to propose the mechanism for the $TPPBF_4$–Bip-cosensitized PET oxygenation reactions leading to **4** as shown in Scheme 3. SET oxidation of **5** with the excited singlet state of $TPPBF_4$ leads to generate the corresponding cation radical $\mathbf{5}^{+\cdot}$, which cyclyzes to generate the *o*-xylylene cation radical $\mathbf{7}^{+\cdot}$ [27, 28]. Reaction of $\mathbf{7}^{+\cdot}$ with molecular oxygen ($^3O_2$) followed by back electron transfer from pyryl radical (TPP$^\cdot$) or electron transfer from **5** then affords **4**. Under the irradiation condition, *o*-diaroylbenzene **6** is produced by SET from **4** to the excited singlet state of $TPPBF_4$ [42]. Our previous result that **4a** was formed in the tris(4-bromophenyl)aminium hexachloroantimonate-catalyzed oxygenation of **5a** under oxygen in the dark supports the participation of $^3O_2$ in this $TPPBF_4$-sensitized PET oxygenation reactions [28]. The possibility of involvement of oxygen anion radical ($O_2^{-\cdot}$) in the oxygenation process can be ruled out by taking into account the redox properties of the excited $TPPBF_4$ [30, 40, and 43–46]. Electron transfer from TPP$^\cdot$ to $^3O_2$ is calculated to be endothermic by approximately 20.1 kcal mol^{-1} using the reduction potentials ($E_{1/2}^{OX}$) of –0.43 V and –1.30 V (*vs.* SCE in CH_3CN) respectively for $TPPBF_4$ and $^3O_2$. Thus, generation of $O_2^{-\cdot}$ by this electron transfer step is unfavorable. On the other hand, participation of singlet oxygen ($^1O_2$) in this oxygenation process is also unfavorable because the generation of $O_2^{-\cdot}$ and $^1O_2$ can be ruled out as reported in the $TPPBF_4$-sensitized PET oxygenation reaction of adamantylideneadamantane [47]. The efficiency enhancement effect of addition of Bip ($E_{1/2}^{OX}$ = +1.86 V *vs.* SCE in CH_3CN) to the reaction mixture, while not being fully elucidated at the present stage owing to the lack of spectroscopic data, is likely a consequence of the

participation of Bip in electron transfer with the excited singlet state of $TPPBF_4$ that takes place in addition to electron transfer from **5** to generate Bip cation radical ($Bip^{+\cdot}$) [48]. This leads to a greater utilization of the excited state of $TPPBF_4$ in forming cation radical species that eventually produce the key reactive intermediate $\mathbf{5}^{+\cdot}$. Thus, under the $TPPBF_4$–Bip-cosensitized conditions $\mathbf{5}^{+\cdot}$ is effectively generated by exothermic electron transfer from **5** to $Bip^{+\cdot}$. Under the DCA-sensitized photoreaction conditions, oxygenation pathways similar to those involved in the $TPPBF_4$–Bip-cosensitized process take place except that $O_2^{-\cdot}$ and $^1O_2$ are also produced as reactive intermediates [48–50].

(Scheme 3)

The in vitro antimalarial activities of endoperoxides **4a-d** against *Plasmodium falciparum* (*P. falciparum*) and their cytotoxicities against mouse mammary tumor FM3A cells (FM3A cells) were evaluated in order to clarify relationships that may exist between activities and the nature of aromatic substituents (Table 2) [6, 7, and 9]. The results show that EC_{50} of **4a-d** against *P. falciparum* are in the range of 1.7×10^{-7} to 8.0×10^{-8} M, values that are higher than those of **1a-d** (1.2×10^{-6} - 5.6×10^{-7} M) [13]. The nature of the benzo-substituent in **4a-d** remarkably influence antimalarial activities of **4a-d**, which may be a consequence of their enhances of lipophilicities compared with **1a-d**. In addition, fairly high antimalarial activities and selectivities (cytotoxicity against FM3A cells/antimalarial activity against *P. falciparum*: see Experimental Section) are displayed by **4c** and **4d**. The high antimalarial activities and low toxicities of **4c** and **4d** may be the results of the presence of 1,4-disubstituted electron-donating aromatic groups as compared to those in **4a** and **4b**. The activities of **4a** and **4b** are somewhat lower and their selectivities are poor owing to their slightly high toxicities. Although the presence of a fluorine atom in **1** and **2** has been reported to enhance antimalarial activities [10], the activity of **4b** dose not reflect this effect. Finally, in spite of their structural and synthetic simplicities, the new series of benzo-fused bicyclic peroxides **4a-d** should serve as promising lead compounds in efforts targeted at the design and preparation of new antimalarial drugs.

(Table 2)

Conclusion

In conclusion, the results of the investigation described above demonstrate that benzo-fused bicyclic peroxides **4a-d** can be efficiently prepared by utilizing $TPPBF_4$–Bip-cosensitized PET oxygenation processes. The $TPPBF_4$–Bip-cosensitized PET oxygenation reaction should serve as a convenient method to synthesize various antimalarial cyclic peroxides through concise sequences owing to the fact that it enables introduction of an O–O bond simultaneous with C–C bond formation in certain dienes [17] or C–C bond cleavage in certain cyclopropanes [51]. We are now investigating further structural modifications of these substances and the Fe(II)-promoted degradation of **4** with the aim of clarifying the relationship that might exist between reaction intermediates and antimalarial activities.

Experimental

General experimental procedures

All melting points are uncorrected. Elemental analyses were performed at the Research and Analytical Center for Giant Molecules, Graduate School of Science, Tohoku University. ^1H and ^{13}C NMR spectra were recorded on a Varian Gemini-200 Spectrometer (operating at 200 MHz for ^1H and 50 MHz for ^{13}C) using $CDCl_3$ as solvent. Half-wave oxidation potentials were measured on a BAS cyclic voltammograph CV-1B. CH_3CN (Wako, special grade) for electrochemical measurements and photoreactions was distilled twice over phosphorus(V) oxide and once over calcium hydride. Triphenyl pyrilium tetrafluoroborate ($TPPBF_4$) was prepared by the reported method [52] and recrystallized twice from CH_3CN. 9,10-Dicyanoanthracene (DCA, Wako) was recrystallized from CH_3CN.

*Photo-oxygenation of 1,2-bis(1-arylethenyl)benzenes **5a-d** using SET sensitizers*

An oxygen-purged CH_3CN (10 ml) solution of **5** (0.20 mmol) and a catalytic amount of $TPPBF_4$ (0.02 mmol) or DCA (0.002 mmol) in the presence or absence of Bip (0.60 mmol) was irradiated ($\lambda > 360$ nm) using a 2-kW Xe lamp. The resulting mixture was concentrated

and the residue was subjected to silica gel TLC separation (*n*-hexane/CH_2Cl_2) to afford the benzo-fused bicyclic peroxide **4** as a major product and a small amount of *o*-diaroylbenzene **6**. The structures of **4a-d** were determined by analysis of their spectroscopic data and comparisons of the data with those reported for **4a** [27].

Compound **4a**: colorless needles; mp 192–194 °C (CH_3OH); IR (KBr, cm^{-1}) 3090, 3060, 2970, 2884, 1606, 1498, 1248, 1045; ^1H NMR (200 MHz, $CDCl_3$), δ: 2.27–2.52 (m, 2H), 2.71–2.96 (m, 2H), 6.68–6.78 (m, 2H), 7.18–7.28 (m, 2H), 7.35–7.70 (m, 10H); ^{13}C NMR (50 MHz, $CDCl_3$), δ: 28.3 (t, 2C), 80.7 (s, 2C), 122.9 (d, 2C), 127.1 (d, 4C), 127.8 (d, 2C), 128.4 (d, 4C), 128.6 (d, 2C), 137.0 (s, 2C), 140.7 (s, 2C). Anal. calcd for $C_{22}H_{18}O_2$: C, 84.05; H, 5.77. Found: C, 83.71; H, 5.84. MS (EI) *m/z* 314 (M^+, 2%), 282 (100%).

Compound **4b**: colorless needles; mp 222–224 °C (C_2H_5OH); IR (KBr, cm^{-1}) 3090, 2975, 2900, 1607, 1504, 1222, 1051; ^1H NMR (200 MHz, $CDCl_3$), δ: 2.22–2.48 (m, 2H), 2.68–2.87 (m, 2H), 6.65–6.78 (m, 2H), 7.10–7.32 (m, 6H), 7.48–7.63 (m, 4H); ^{13}C NMR (50 MHz, $CDCl_3$), δ: 28.3 (t, 2C), 80.4 (s, 2C), 115.4 (d, 4C, $J_{C\text{-}F}$ = 21.8 Hz), 122.8 (d, 2C), 128.0 (d, 2C), 129.1 (d, 4C, $J_{C\text{-}F}$ = 8.3 Hz), 132.7 (d, 2C, $J_{C\text{-}F}$ = 3.1 Hz), 140.5 (s, 2C), 162.8 (s, 2C, $J_{C\text{-}F}$ = 247 Hz). Anal. calcd for $C_{22}H_{16}F_2O_2$: C, 75.42; H, 4.60. Found: C, 75.20; H, 4.70. MS (EI) *m/z* 350 (M^+, 1%), 318 (100%).

Compound **4c**: colorless prisms; mp 224–226 °C (C_2H_5OH); IR (KBr, cm^{-1}) 3010, 2945, 2905, 2830, 1607, 1508, 1238, 1038; ^1H NMR (200 MHz, $CDCl_3$), δ: 2.25–2.45 (m, 2H), 2.42 (s, 6H), 2.73-2.86 (m, 2H), 6.68–6.78 (m, 2H), 7.16–7.32 (m, 6H), 7.40–7.48 (m, 4H): ^{13}C NMR (50 MHz, $CDCl_3$), δ: 21.3 (q, 2C), 28.2 (t, 2C), 80.7 (s, 2C), 122.9 (d, 2C), 127.1 (d, 4C), 127.7 (d, 2C), 129.1 (d, 4C), 134.0 (s, 2C), 138.4 (s, 2C), 140.9 (s, 2C). Anal. calcd for $C_{24}H_{22}O_2$: C, 84.18; H, 6.48. Found: C, 84.04; H, 6.53. MS (EI) *m/z* 342 (M^+, 2%), 310 (100%).

Compound **4d**: colorless needles; mp 206–208 °C (C_2H_5OH); IR (KBr, cm^{-1}) 3040, 3010, 2897, 1596, 1513, 1259, 1034; ^1H NMR (200 MHz, $CDCl_3$), δ: 2.14–2.46 (m, 2H), 2.69–2.98 (m, 2H), 3.87 (s, 6H), 6.72–6.80 (m, 2H), 6.97–7.07 (m, 4H), 7.17–7.30 (m, 2H), 7.45–7.55 (m, 4H): ^{13}C NMR (50 MHz, $CDCl_3$), δ: 28.1 (t, 2C), 55.3 (q, 2C), 80.5 (s, 2C), 113.7 (d, 4C), 122.9 (d, 2C), 127.6 (d, 2C), 128.7 (d, 4C), 128.9 (s, 2C), 141.0 (s, 2C), 159.7 (s, 2C). Anal. calcd for $C_{24}H_{22}O_4$: C, 76.99; H, 5.92. Found: C, 76.64; H, 5.95. MS (EI) *m/z* 374 (M^+, 8%), 342 (100%).

In vitro antimalarial activities of benzo-fused 1,4-diaryl-2,3-dioxabicyclo[2.2.2]octanes ***4a-d***

Plasmodium falciparum (ATCC 30932, FCR-3 strain) was used in this study. *P. falciparum* was cultivated by a modification of the method of Trager and Jensen [53] using a 5% hematocrit of type A human red blood cells suspended in RPMI 1640 medium (Gibco, NY) supplemented with heat-inactivated 1% type A human serum. The following procedures were used for assay of antimalarial activity. Asynchronously cultivated *P. falciparum* were used. Various concentrations of **4a-d** in dimethyl sulfoxide were prepared. 5 μL of each solution was added to individual wells of a multidish, 24 wells. Erythrocytes with 0.3% parasitemia were added to each well containing 995 μL of culture medium to give a final hematocrit level of 3%. The plates were incubated at 37 °C for 72 h in a CO_2-O_2-N_2 incubator (5% CO_2, 5% O_2, and 90% N_2 atmosphere). To evaluate the antimalarial activity of test compound, we prepared thin blood films from each culture and stained them with Giemsa (E. Merck, Germany). Total 1 X 10^4 erythrocytes/1 thin blood film were examined under microscopy. All of the test compounds were assayed in duplicate at each concentration. Drug-free control cultures were run simultaneously. All data points represent the mean of three experiments. Parasitemia in control reached between 4% and 5% at 72 h. The EC_{50} value refers to the concentration of the compound necessary to inhibit the increase in parasite density at 72 h by 50% of control.

Toxicity against mammalian cell line

Mouse mammary tumor FM3A cells (wild-type, subclone F28-7) were supplied by the Japanese Cancer Research Resources Bank (JCRB). FM3A cells were maintained in suspension culture at 37 °C in a 5% CO_2 atmosphere in plastic bottles containing ES medium (Nissui Pharmaceuticals, Japan) supplemented with 2% heat-inactivated fetal bovine serum (Gibco, NY). FM3A cells grew with a doubling time of about 12 h. Prior to exposure to drugs, cell density was adjusted to 5 X 10^4 cells/mL. A cell suspension of 995 μL was dispensed to the test plates, and compound at various concentrations suspended in dimethyl sulfoxide (5 μL) was added to individual wells of a multidish, 24 wells. The plates were incubated at 37 °C in a 5% CO_2 atmosphere for 48 h. All of the test compounds were assayed in duplicate at each concentration. Cell numbers were measured using a microcell counter CC-130 (Toa Medical Electric Co., Japan). All data points represent the mean of three experiments. The

EC_{50} value refers to the concentration of the compound necessary to inhibit the increase in cell density at 48 h by 50% of control. Selectivity refers to the mean of EC_{50} value for FM3A cells per the mean of EC_{50} value for *P. falciparum*.

Acknowledgments. We gratefully acknowledge financial support provided by The Uchida Energy Science Promotion Foundation. We also thank Professor Eietsu Hasegawa (Department of Chemistry, Faculty of Science, Niigata University), Professor Ryoichi Akaba (Department of Chemistry, Gunma College of Technology), Professor Tsutomu Miyashi (Department of Chemistry, Graduate School of Science, Tohoku University), Professor Yasutake Takahashi (Graduated School of Medicine and Pharmaceutical Science for Education, University of Toyama), and Professor Hiroshi Ikeda (Department of Chemistry, Graduate School of Engineering, Osaka Prefecture University) for their helpful comments and assistance.

References

1. S.R. Meshnick, C.W. Jefford, G.H. Posner, M.A. Avery, W. Peters, Parasitol. Today, **12**, 79-82 (1996) and references cited therein
2. K.J. McCullough, M. Nojima, Curr. Org. Chem. **5**, 601-636 (2001)
3. A.J. Bloodworth, T. Hagen, K.A. Johnson, I. Lenoir, C. Moussy, Tetrahedron Lett. **38**, 635-638 (1997)
4. P.M. O'Neil, L.P. Bishop, N.L. Searle, J.L. Maggs, S.A. Ward, P.G. Bray, R.C. Storr, B.K. Park, Tetrahedron Lett. **38**, 4263-4266 (1997)
5. Y. Takaya, K. Kurumada, Y. Takeuji, H.-S. Kim, Y. Shibata, N. Ikemoto, Y. Wataya, Y. Ohshima, Tetrahedron Lett. **39**, 1361-1364 (1997)
6. H.-S. Kim, Y. Shibata, Y. Wataya, K. Tsuchiya, A. Masuyama, M. Nojima, J. Med. Chem. **42** 2604 -2609 (1999)
7. H.-S. Kim, Y. Nagai, K. Ono, K. Begum, Y. Wataya, Y. Hamada, K. Tsuchiya, A. Masuyama, M. Nojima, K. J. McCullough, J. Med. Chem. **44**, 2357-2361 (2001)
8. S.H. Hindley, S.A. Ward, R.C. Storr, N.L. Searle, P.G. Bray, B.K. Park, J. Davies, P.M. O'Neil, J. Med. Chem. **45**, 1052-1063 (2002)

9. Y. Hamada, H. Tokuhara, A. Masuyama, M. Nojima, H.-S. Kim, K. Ono, N. Ogura, Y. Wataya, J. Med. Chem. **45**, 1374-1378 (2002) and references cited therein
10. G.H. Posner, X. Tao, J.N. Cumming, D. Klinedinst, T.A. Shapiro, Tetrahedron Lett. **37**, 7225-7228 (1996)
11. G.H. Posner, D. Wang, L. Gonzares, X. Tao, J.N. Cumming, D. Klinedinst, T.A. Shapiro, Tetrahedron Lett. **37**, 815-818 (1996)
12. G.H. Posner, L. Gonzares, J.N. Cumming, D. Klinedinst, T.A. Shapiro, Tetrahedron **53**, 37-50 (1997)
13. M. Kamata, T. Kudoh, J. Kaneko, H.-S. Kim, Y. Wataya, Tetrahedron Lett. **43**, 617-620 (2002)
14. M. Kamata, C. Satoh, H.-S. Kim, Y. Wataya, Tetrahedron Lett. **43**, 8313-8317 (2002)
15. Y. Takahashi, K. Wakamatsu, S. Morishima, T. Miyashi, J. Chem. Soc., Perkin Trans. 2, 243-253 (1993)
16. M. Suzuki, H. Ohtake, Y. Kameya, N. Hamanaka, R. Noyori, J. Org. Chem. **54**, 5292-5302 (1989)
17. M. Kamata, M. Ohta, K. Komatsu, H.-S. Kim, Y. Wataya, Tetrahedron Lett. **44**, 2063 -2067 (2002)
18. M. Kamata, K. Murayama, T. Miyashi, Tetrahedron Lett. **31**, 4129-4132 (1989)
19. M. Kamata, K. Murayama, T. Miyashi, J. Chem. Soc., Chem. Commun. 828-829 (1990)
20. M. Kamata, Y. Kato, E. Hasegawa, Tetrahedron Lett. **32**, 4349-4352 (1991)
21. M. Kamata, H. Otogawa, E. Hasegawa, Tetrahedron Lett. **32**, 7421-7424 (1991)
22. M. Kamata, M. Sato, E. Hasegawa, Tetrahedron Lett. **33**, 5085-5088 (1992)
23. M. Kamata, Y. Murakami, Y. Tamagawa, M. Kato, E. Hasegawa, Tetrahedron **45**, 12821-12828 (1994)
24. M. Kamata, Y. Yokoyama, N. Karasawa, M. Kato, E. Hasegawa, Tetrahedron Lett. **37**, 3483-3486 (1996)
25. M. Kamata, S. Nagai, M. Kato, E. Hasegawa, Tetrahedron Lett. **37**, 7779-7782 (1996)
26. M. Kamata, K. Komatsu, R. Akaba, Tetrahedron Lett. **42**, 9203-9206 (2001)
27. Y. Takahashi, Y. Ohya, H. Ikeda, T. Miyashi, J. Chem. Soc., Chem. Commun. 1749 -1750 (1995)
28. H. Ikeda, T. Ikeda, M. Akagi, H. Namai, T. Miyashi, Y. Takahashi, M. Kamata, Tetrahedron Lett. **46**, 1831-1835 (2005)

29. W.Y. Lee, B.G. Moon, C.-H. Park, S.-H. Bang, J.H. Lee, Bull. Korean Chem. Soc. **9**, 325-328 (1988)
30. M.A. Miranda, H. Garcia, Chem. Rev. **94**, 1063-1089 (1994) and references cited therein.
31. D. Rehm, A. Weller, Isr. J. Chem. **8**, 259 (1970)
32. M.A. Fox, M. Chanon, Eds., *Photoinduced Electron Transfer,* Elsevier, Amsterdam, Parts A-D, (1988)
33. P.S. Mariano, Ed., *Advances in Electron Transfer Chemistry*, JAI Press, Greenwich, Vols 1-6, (1991-1999)
34. V. Balzani, Ed., *Electron Transfer in Chemistry*, WILEY-VCH, Weinheim, Vols 1-5, (2001)
35. A.P. Schaap, S. Siddiqui, G. Prasad, E. Palomino, M. Sandison, Tetrahedron, **41**, 2229-2235 (1985)
36. A.P. Schaap, L. Lopez, S.D. Gagnon, J. Am. Chem. Soc. **105**, 663-664 (1983)
37. A.P. Schaap, S. Siddiqui, S.D. Gagnon, L. Lopez, J. Am. Chem. Soc. **105**, 5149 -5150 (1983)
38. A.P. Schaap, L. Lopez, S.D. Anderson, S.D. Gagnon, Tetrahedron Lett. **22**, 5493-5496 (1982)
39. T. Miyashi, H. Ikeda, A. Konno, O. Okitsu, Y. Takahashi, Pure Appl. Chem. **62**, 1531-1538 (1990)
40. A.G. Griesbeck, O. Sadlek, K. Polborn, Liebigs Ann. 545-549 (1996)
41. Y. Takahashi, O. Okitsu, M. Ando, T. Miyashi, Tetrahedron Lett. **35**, 3953-3956 (1994)
42. M. Kamata, J. Kaneko, J. Hagiwara, R. Akaba, Tetrahedron Lett. **45**, 7423-7428 (2004)
43. R. Akaba, H. Sakuragi, K. Tokumaru, J. Chem. Soc., Perkin Trans. 2, 291-297 (1991)
44. G. Haucke, P. Czerney, F. Cebulla, Ber. Bunsen-Ges. Phys. Chem. **96**, 880-886 (1992)
45. S.L. Mattes, S. Farid, Acc. Chem. Res. **15**, 80-86 (1982)
46. S.L. Mattes, S. Farid, In *Organic Photochemistry*, A. Padwa, Ed., Marcel Dekker, New York, Vol.6, Chap.4 (1983)
47. R.Akaba, S.Aihara, H.Sakuragi, K.Tokumaru. J. Chem. Soc., Chem. Commun. 1262-1263 (1987)
48. I.R. Gould, D. Ege, J.E. Moser, S. Farid, J. Am. Chem. Soc. **112**, 4290-4301 (1990) and references cited therein
49. L.E. Marning, C. Gu, C.S. Foote, J. Phys. Chem. **87**, 40-44 (1983)

50. J. Santamaria, Tetrahedron Lett. **22**, 4511-4514 (1981)

51. M. Kamata, Y. Nishikata, M. Kato, J. Chem. Soc., Chem. Commun. 2047-2048 (1996)

52. J.A. VanAllan, G.A. Reynolds, J. Org. Chem. **33**, 1102-1105 (1968)

53. W. Trager, J.B. Jensen, Science **193**, 673-675 (1976)

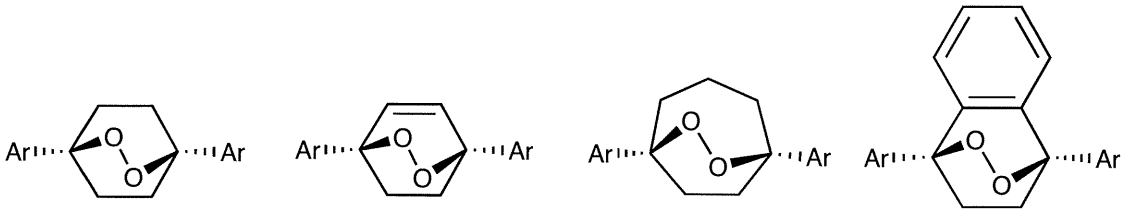

1 **2** **3** **4**

a: Ar = C_6H_5
b: Ar = *p*-FC_6H_4
c: Ar = *p*-MeC_6H_4
d: Ar = *p*-$MeOC_6H_4$

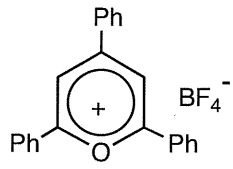

TPPBF$_4$

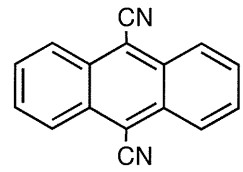

DCA

Scheme 1